CHIN. PHYS. LETT. Vol. 35, No. 3 (2018) 034202

Beam Steering Analysis in Optically Phased Vertical Cavity Surface Emitting Laser Array *

Meng Xun(荀孟)[1**], Yun Sun(孙昀)[1], Chen Xu(徐晨)[2], Yi-Yang Xie(解意洋)[2], Zhi Jin(金智)[1], Jing-Tao Zhou(周静涛)[1], Xin-Yu Liu(刘新宇)[1], De-Xin Wu(吴德馨)[1]

[1]*Institute of Microelectronics, Chinese Academy of Sciences, Beijing 100083*
[2]*Key Laboratory of Optoelectronics Technology (Ministry of Education), Beijing University of Technology, Beijing 100124*

(Received 10 October 2017)

Beam steering in implant defined coherently coupled vertical cavity surface emitting laser (VCSEL) arrays is simulated using the FDTD solution software. Angular deflection dependent on relative phase differences among elements, inter-element spacing, element size and emitted wavelength is analyzed detailedly and systematically. We design and fabricate 1×2 implant defined VCSEL arrays for optimum beam steering performance. Electronically controlled beam steering with a maximum deflection angle of 1.6° is successfully achieved in the 1×2 VCSEL arrays. The percentage of the power in the central lobe is above 39% when steering. The results show that the steering is controllable. Compared with other beam steering methods, the fabrication process is simple and of low cost.

PACS: 42.55.Px, 61.72.uj, 42.25.Ja DOI: 10.1088/0256-307X/35/3/034202

Beam steering is important for a wide range of applications,[1–3] including signal processing, display, laser scanning and free-space interconnection. Mechanical methods limit steering speed, sizes and lifetime.[4,5] Non-mechanical methods are more sensitive and more reliable, which are very important for laser radar application. To achieve the goal, several methods have been proposed. In-plane liquid crystal devices with a separation structure realized beam steering.[6] Output-beam scanning and switching characteristics in lasers were achieved via separately controlled twin-stripe electrodes.[7] Beam direction was controlled via semiconductor lasers using two-dimensional photonic crystals with triangular air holes.[8]

A new method to achieve beam steering is via coherently coupled vertical cavity surface emitting laser (VCSEL) arrays. An independent injection current into every element varied the relative phase between elements and caused electronic beam steering in the far-field profile. The coherently coupled VCSEL arrays were fabricated by the proton implantation process.[9–11] The beam steering in implant defined VCSEL arrays was firstly reported by Lehman *et al.*[12] Johnson *et al.* analyzed the phase extraction from a phase array.[13] It should be noted that the deflection angle and the beam quality in steering are affected by many array parameters. It is therefore important to understand the influence of these parameters on steering characteristics. There are few, if any, studies discussing the optimization of VCSEL arrays for beam steering in this respect. In this work, we study the effect of relative phase difference between elements, inter-element spacing, element width and emitted wavelength on deflection angle, divergence and side lobe intensity. We use the FDTD solution software to simulate the far-field variation of coherently coupled arrays. In addition, we design and fabricate 1 × 2 implant defined coherently coupled VCSEL arrays. Novel contacts are designed to make the current injection controllable into each element. The maximum deflection angle is 1.6°. Controllable and highly coherent beam steering is achieved successfully.

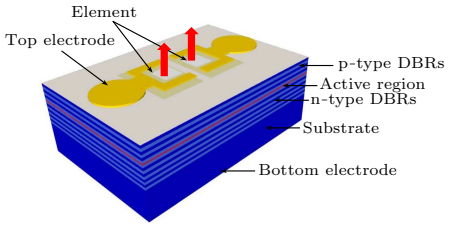


Fig. 1. Schematic structure of a 1 × 2 VCSEL array for beam steering.

In the implant defined VCSEL arrays, the refractive index is affected by both thermal and carriers. Thus the index profile across the active region varies with the current injection. Therefore, the phase of each element can be controlled by the current injection separately. A schematic structure of a 1 × 2 beam steering VCSEL array is shown in Fig. 1. To investigate properties of beam steering in the VCSEL arrays, we use FDTD solution software based on the finite difference method to simulate beam steering. The model consists of DBRs and the active region. The size of the model is the same as actual devices. The virtual

*Supported by the 'Supporting First Action' Joint Foundation for Outstanding Postdoctoral Program under Grant Nos Y7YBSH0001 and Y7BSH14001, the National Natural Science Foundation of China under Grant No 61434006, and the National Key Basic Research Program of China under Grant No 2017YFB0102302.

**Corresponding author. Email: xunmeng@ime.ac.cn

© 2018 Chinese Physical Society and IOP Publishing Ltd

light sources in each element are set to be of Gaussian distribution, emitting from the active region into top DBRs. The perfect matched layer (PML) boundary condition is employed.

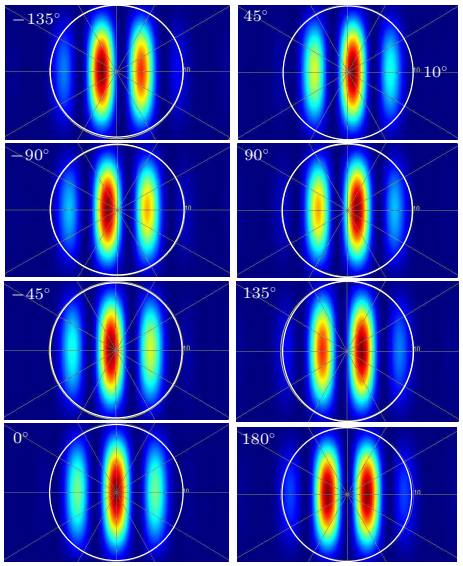


Fig. 2. Simulated far-field profiles of 1×2 arrays with different element phases.

Firstly, we investigate the angular deflection dependent on the relative phase difference (ϕ). In the simulation, the size of the element (w) is 6 μm × 6 μm and the inter-element spacing(s) between elements is 4 μm. The emitted wavelength λ is set as 850 nm. The simulated far-field profiles of 1 × 2 arrays of different phase differences are shown in Fig. 2. The greater the relative phase difference between the two elements is, the larger the shifted angle in the far-field profile is. An in-phase coupled far-field profile appears when the elements are of the same phase. When the phase difference is above 90°, there are two lobes in the far-field profiles apparently. An out-of-phase mode occurs when there is 180° phase difference between elements. The deflection angles and the intensity ratio between lobes in far-field profiles versus the relative phase difference between elements are carried out in Fig. 3. From this date, the deflection angle varies linearly with the relative phase difference. The intensity ratio between the main lobe and the side lobes reaches a maximum of 2.05 while the two elements are in-phase with each other. The intensity in side lobes increases when there is a relative phase difference between elements and therefore the intensity ratio decreases, which indicates that the angular deflection lowers the intensity contrast.

Inter-element spacing is an important factor influencing angular deflection in far-field profiles. In this simulation, the size of the element is 6 μm × 6 μm and the emitted wavelength is 850 nm. The phase difference between the elements is fixed to a constant of 90°. Figure 4(a) shows the simulated 1D far-field profiles with different inter-element spacings. It shows that the peak of the far-field profile shifts to the left when the inter-element varies from 2 μm to 6 μm. From this, we may conclude that the angular deflection decreases with increasing the inter-element spacing. Therefore, to achieve a larger angular shift in the far-field patterns at a fixed phase difference between elements, decreasing inter-element spacing between elements is required. However, in the practical fabrication process, a very small inter-element spacing is hard to achieve because of the inaccuracy in etching and lithography. With the improvement of the fabrication process, it is possible to compress the intensity of side lobe in the future. In addition, the modal properties dependent on inter-element spacing must be accounted for in the VCSEL array design. According to our previous results, the in-phase mode is radiated as the inter-element spacing is from 2 μm to 4 μm.[14] Thus the inter-element spacing was chosen as 2 μm for considering both the steering angle and the array mode.

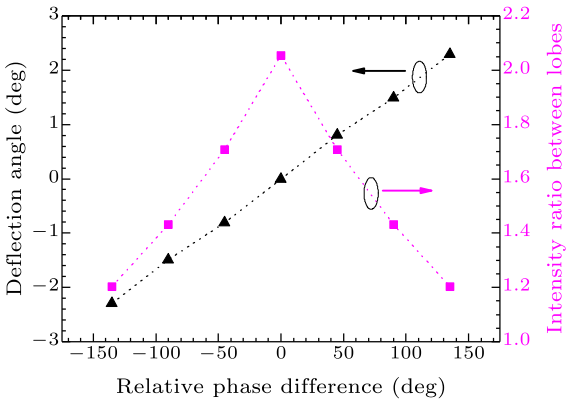


Fig. 3. Deflection angle and intensity ratio between lobes in far-field profiles versus the relative phase difference between elements.

The far-field profiles dependent on the width of elements are also simulated as shown in Fig. 4(b). The center-to-center distance is a constant of 10 μm. The emitted wavelength is 850 nm and the relative phase difference is 90°. It is clear that the increase of the element width just reduces the intensity peak of side lobes, and makes no change to the steering angle. Enlarging the element width can concentrate more power in the central lobe. It is important to lower the intensity of side lobe power to increase the distinguishing ability. However, for a single VCSEL emitter, enlarging the width typically makes the higher-order mode radiate. It is necessary to keep a fundamental mode operation in elements to achieve in-phase mode in the coherent arrays. Thus the width of the elements is chosen as 7 μm in our experiment to lower the intensity of side lobes and to avoid a higher-order mode to be radiated from each element. The far-field profiles dependent on emitted wavelength analysis was also undertaken, as shown in Fig. 4(c). The inter-element spacing is kept to be 4 μm and the size of the ele-

ment is 6 μm × 6 μm. It is obvious that the peak of far-field profiles shifts to the right while the emitted wavelength increases. Increasing wavelength is an alternative to obtain a larger deflection angle. Table 1 summarizes the deflection angle varying with different array parameters.

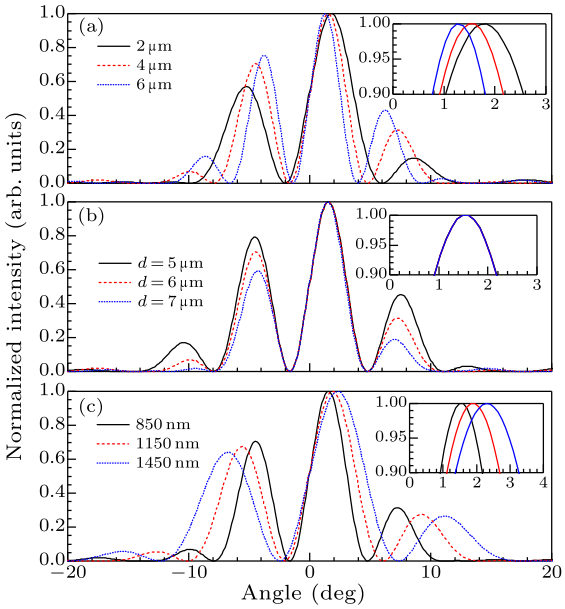


Fig. 4. (a) Simulated 1D far-field profiles of arrays with different inter-element spacings, (b) widths of elements, and (c) emitted wavelengths.

We fabricated the implant defined VCSEL arrays. The epitaxial structure with 850 nm wavelength was grown on a good uniform n-GaAs substrate by mental organic chemical vapor deposition (MOCVD). The structure consists of 22.5 pairs of p-type top DBRs and 34.5 pairs of n-type bottom DBRs. The quantum well is GaAs and the barrier layer is $Al_{0.3}Ga_{0.7}As$. The concentration in the top layer is $1.9 \times 10^{19}/cm^3$ to form ohmic contact. The process used to form an implant-defined VCSEL array was as follows. Firstly, thick SiO_2 was deposited on the surface of the wafer using PECVD. The proton implantation resist masks were made by inductively coupled plasma etching. The peak implant damage is usually designed to occur somewhat above the quantum wells to avoid excessive damage to the active medium. A 315 keV proton implantation with a dose of $1 \times 10^{15}/cm^3$ was employed for the VCSEL array. To avoid ion channeling during implantation, the samples were inclined by 7° from normal. To electrically isolate an element from the other element, multiple stacked implants with successively decreased energy were made. Next, the proton-implantation resist masks were removed. A novel contact was designed to make possible the control of current injection into each element separately. The novel contact consists of an Au nano layer and separated Ti/Au electrodes. The Au nano layer was used to form the current route from electrodes to elements. Finally, AuGeNi/Au was deposited on the GaAs substrate to form the cathode.

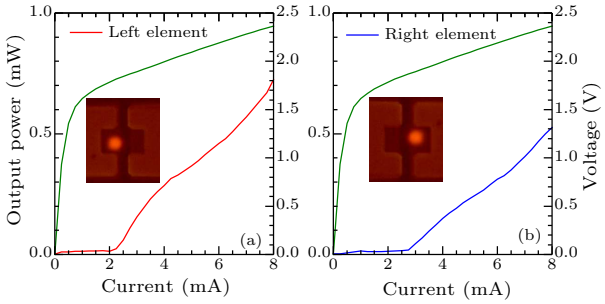


Fig. 5. The P–I–V curves of (a) left element and (b) right element with current injection to only one element. Insets: corresponding near-field profiles, showing sufficient isolation between elements.

The current-voltage-power characteristics of two elements with respective current injections (I_L and I_R) are shown in Fig. 5. The corresponding near-field profiles measured by a CCD camera are shown in the insets. It can be seen that the injected current was restricted to its aperture, indicating that effective isolation between the elements was achieved. The resistance between the left and right contacts is about $1.6 \times 10^6\,\Omega$. The threshold of the left element is 2.25 mA. The series resistance of the left element is 101.31 Ω under the current of 4 mA. The threshold of the right element is 2.75 mA. The series resistance of the right element is 101.78 Ω under the current of 4 mA. The two elements were initially designed to be the same. The difference may come from misalignments during photolithography and non-uniformity in the etching process. Thus the peak of the far-field profile may not be on-axis because of the difference between the two elements. By independent current injecting into each element, the peak location of the far-field profile can be varied.

Table 1. Deflection angle variation with different array parameters.

Array parameters	$w = 6\,\mu m$, $\lambda = 850\,nm$, $\phi = 90°$, Inter-element spacing (μm)			$s = 6\,\mu m$, $\lambda = 850\,nm$, $\phi = 90°$, element width (μm)			$w = 6\,\mu m$, $s = 4\,\mu m$, $\phi = 90°$, wavelength (nm)		
	2	4	6	5	6	7	850	1150	1450
Deflection angle (deg)	1.25	1.55	1.8	1.55	1.55	1.55	1.55	1.9	2.3

Figure 6(c) shows the schematic of the experimental setup for near-field and far-field measurements. The device was driven under continuous conditions by two separate current sources. Near-field and far-field profiles were measured for current values I_L and I_R injected into the left and right contacts. When $I_L = 3.9$ mA and $I_R = 4.1$ mA, a generated in-phase coherently coupled near-field profile and far-field pro-

file are shown in Figs. 6(a) and 6(b), respectively. There is one dominant lobe in the far-field profile. The full width at half maximum (FWHM) is only 2.4°. The intensity of central lobe is above 1.77 times as high as that of any subsidiary lobes. Approximately 44.6% of total power is localized in the central lobe. This indicates that the two elements have nearly equal phases.

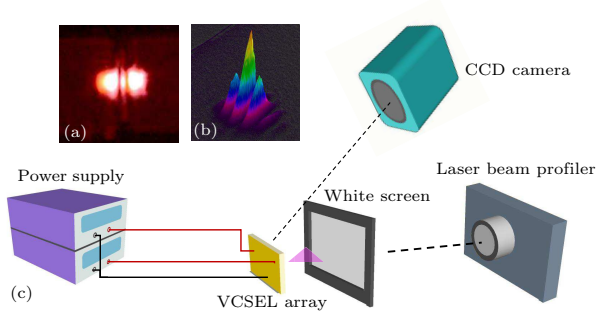


Fig. 6. Current injected to both the elements producing coherent (a) near-field profile and (b) far-field profile. (c) Schematic diagram of experimental setup.

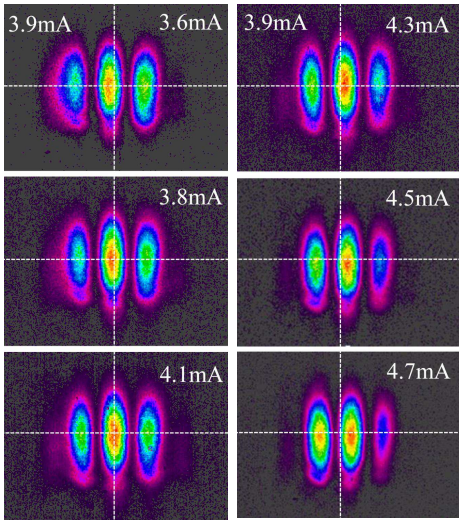


Fig. 7. Measured far-field profiles of the 1×2 arrays under different combinations of current values.

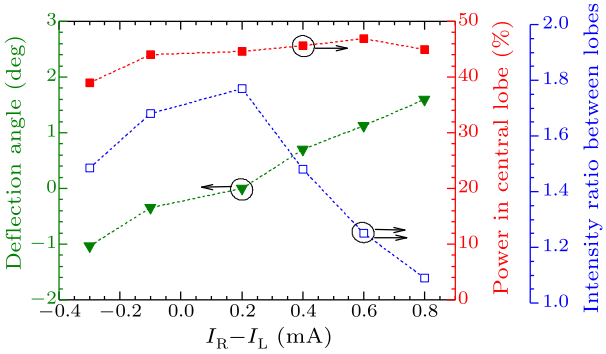


Fig. 8. Defection angle, power in central lobe and intensity ratio between lobes in far-field profiles versus $I_R - I_L$.

Then we investigated the function of beam steering of the 1×2 coherently coupled arrays. The peak of far-field profiles can be varied via independent currents injected into each element. The current (I_R) injected into the right element varies from 3.5 mA to 4.5 mA. The current (I_L) injected into the left element maintains a constant of 3.9 mA ($1.7I_{th}$). The measured far-field profiles of the array under different combinations of current values are shown in Fig. 7. It can be observed apparently that the beam moves in two directions. When I_R is above 4.1 mA, the peak of the central lobe in the far-field profile moves towards the right. When I_R is below 4.1 mA, the peak of the central lobe in the far-field profiles moves towards the left. The results indicate that the control of beam steering is achieved successfully. The deflection angle of the peak of the central lobe in the far-field profile versus $I_R - I_L$ is shown in Fig. 8. The deflection angle is nearly linear with $I_R - I_L$. The trend is the same as the simulated results in Fig. 3. When $I_R - I_L$ is 0.2 mA, the far-field angle deflects 0°. The peak of the far-field profile appears on-axis, which is emitted perpendicular to the surface of the wafer. The intensity ratio between the central lobe and the side lobe is also shown in Fig. 8. The intensity ratio of the central lobe to the side lobe is 1.77 to 1 when $I_R - I_L$ is 0.2 mA. When $I_R - I_L$ is 0.8 mA, the deflection angle reaches a maximum of 1.6°. The intensity ratio of the central lobe to the side lobe is 1.09 to 1. This indicates that the beam quality becomes worse when the angular shift happens. The full-width at half-maximum of the central lobes keeps between 2.4° and 2.7° when steering happens. The power in the central lobes versus $I_R - I_L$ is also shown in Fig. 8. Between 39% and 46% of total power is concentrated in the central lobes. The results show high power in the central lobe with low divergence, which is desirable in practical steering application.

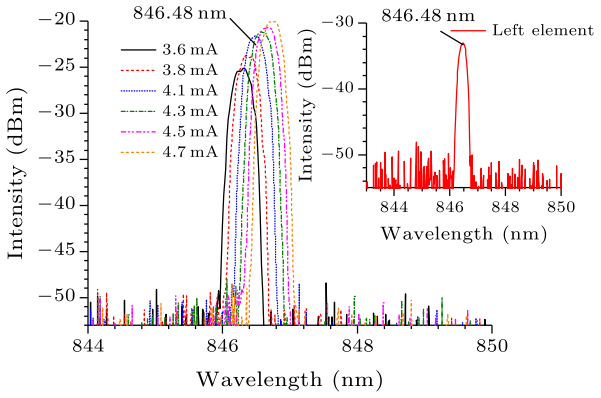


Fig. 9. Measured spectra of the right element at different currents. Inset: measured spectrum of the left element at 3.9 mA.

Figure 9 shows the measured spectra of the right element at different currents using the optical spectrum analyzer (AQ 6370c). The spectrum of the left element at 3.9 mA is shown in the inset. The peak wavelength is 846.48 nm. It can be seen that the right element emits at a smaller wavelength than that of

the left element when the current to the right element is lower than 3.4 mA. Similarly, if the current in the right element is larger than 3.4 mA, the emission from the right element is at a longer wavelength than that of the left element. The emission spectra in the two elements are equal when the current in the right element is 4.1 mA and the current in the left element is 3.9 mA. At this moment, the coherence between the elements is the strongest, which is also obtained from the tested far-field profiles. With the increase of the relative current difference between the elements, the coherence decreases. It is possible that some transitions occur from coupled mode to independent modes in each element.

In summary, we have proved that to obtain a larger deflection angle, except for a larger relative phase difference, decreasing inter-element spacing and increasing emitted wavelength are both needed. The width of elements can only impact the percentage of the total power concentrated in the central lobe. We design and fabricate implant-defined coherently coupled vertical cavity surface emitting laser arrays according to the simulated results. Novel contacts are designed to make currents inject into each element independently. This proves that the beam steering in the coherently coupled arrays is continuous and controllable. The maximum deflection angle in far-field profiles of the 1×2 arrays is 1.6°. The array can maintain a stable and narrow divergence beam, which is desirable for steering applications.

References

[1] Niven G and Mooradian A 2006 *Proc. 13th International Display Workshops LAD2-2* (Otsu, Japan 6–8 December 2006)

[2] Matsuda T, Abe F and Takahashi H 1978 *Appl. Opt.* **17** 878

[3] Wu M C, Solgaard O and Ford J E 2006 *J. Lightwave Technol.* **24** 4433

[4] Kozhenikov M, Basavanhally N R, Weld J D, Low Y L, Kolodner P, Bolle C A, Ryf R, Papazian A R, Olkhovets A, Pardo F, Kim J, Neilson D T, Aksyuk V A and Gates J V 2003 *IEEE Photon. Technol. Lett.* **15** 993

[5] Bishop D J, Giles C R and Austin G P 2002 *IEEE Commun. Mag.* **40** 75

[6] Okada H, Bos P J and Onnagawa H 1998 *Jpn. J. Appl. Phys.* **37** 2576

[7] Mukai S, Watanabe M, Itoh H, Yajima H, Hosoi Y and Uekusa S 1985 *Opt. Quantum Electron.* **17** 431

[8] Kurosaka Y, Iwahashi S, Liang Y, Sakai K, Miyai E, Kunishi W, Ohnishi D and Noda S 2010 *Nat. Photon.* **4** 447

[9] Lehman A C and Choquette K D 2007 *IEEE Photon. Technol. Lett.* **19** 1421

[10] Xun M, Xu C, Xie Y Y, Zhu Y X, Mao M M, Xu K, Wang J, Liu J and Chen H D 2014 *Electron. Lett.* **50** 1085

[11] Xun M, Xu C, Deng J, Xie Y Y, Jiang G Q, Wang J, Xu K and Chen H D 2015 *Opt. Lett.* **40** 2349

[12] Lehman A C, Siriani D F and Choquette K D 2007 *Electron. Lett.* **43** 1203

[13] Johnson M T, Siriani D F, Sulkin J D and Choquette K D 2012 *Appl. Phys. Lett.* **101** 031116

[14] Xun M, Xu C, Xie Y Y, Deng J, Xu K and Chen H D 2015 *IEEE J. Quantum Electron.* **51** 2600106